Appendix G: Finite Element Simulation of Welding Residual Stresses

1 Overview

As described in Section 2, a potential source of over-conservatism in previous engineering critical assessments of the GRW circumferential seam welds was the assumption of yield-magnitude tensile residual stresses. Although a report, commissioned on behalf of GRW, provided X-ray diffraction measurements of the residual stresses in a GRW tanker band joint, the technical review of this report noted possible short-comings and sources of errors in these measurements. Specifically, the sample was extensively cold worked before measurements were made and the measurements were only sub-surface.

In order to provide additional insight into the potential residual stress state in the tanker band joints, TWI has performed a thermo-elastic-plastic finite element simulation of the welding procedure.

2 Objective

- To predict the transverse (axial) welding residual stresses in the GRW tanker band joint by simulating the welding procedure for this joint.

3 Approach

3.1 Geometry

An axisymmetric finite element model of a single band of the GRW tanker band joint was produced in Abaqus/CAE version 6.13-2. The details of the joint geometry are as described in the main report.

For the heat transfer analysis, the finite element mesh was comprised entirely of quadrilateral, linear, 4-node axisymmetric heat transfer elements (type DCAX4 in Abaqus). For the thermal stress analysis, bi-quadratic, axisymmetric, reduced-integration elements were employed. An image of the finite element mesh is shown in Figure G3.

3.2 Material properties

The parent and weld materials as described in a previous technical GRW report (2013) are 5182-H111 and 5183, respectively. Similar alloys also described in (GRW, 2013) are 5083-O and 5182 (or 5183) for the plate and filler wire, respectively. A brief literature review of (Abedrabbo et al, 2007), (AFROX, 2014), (Summers et al, 2014) as well as the online materials databases eFunda (2014) and MatWeb (2014) provided indicative tensile properties. Both materials exhibit relatively similar thermo-mechanical properties. Although room temperature tensile testing has been performed on both parent and weld material samples within the context of the present phase of work, elevated temperature testing was not completed. Therefore, for consistency, tensile properties obtained from literature were employed in the finite element model. The room temperature values used in the finite element simulation (and obtained from literature) are not very different from results obtained from room temperature tensile testing.

The material properties used in the welding simulation are shown in Table G1.

3.3 Loads and boundary conditions

The welding simulation was performed by using a sequential thermal-mechanical analysis. To do so, first a transient heat transfer analysis

was performed in order to obtain the time-dependent temperature distribution. After the heat transfer analysis was completed, the transient temperature field was used to define thermal boundary conditions for a thermal-stress (mechanical) analysis.

For the transient heat transfer analysis, the heat input per weld pass was obtained from calculations based on information contained in the GRW welding procedure document (GRW, 2010). The following assumptions were made:

- The weld pool length, L, is equal to four times the weld pool width (see the shaded region in Figure G3). Specifically, the weld pool width is 9.6mm and the weld pool length is therefore 38.4mm.
- Heating occurs for a time period, τ, equal to the time taken for the weld pool to pass through the model, ie $\tau = L/v$ where v is the travel speed. For the simulations undertaken, v = 73cm/min (or equivalently, v = 12.2mm/sec).
- The heat input provided by the weld is assumed to be ηIV where IV is the welding power (amps multiplied by voltage), and η is the welding process efficiency, assumed to be 0.7.
- During the heating period, the volumetric heating flux should therefore be $Q = \eta IV/AL$, where A is the cross-sectional area of the heated region, approximately 50mm^2.

Based on these assumptions (and the values specified in Table G2), the volumetric heat flux is Q = 2.6 W/mm^3.

Kinematic strain hardening and standard heat loss to the environment were assumed. Convection and radiation thermal boundary conditions were applied to surfaces of the model. The parameters shown in Table G3 were additional used in the finite element model, with the emissivity and convective heat transfer coefficient being based upon TWI's experience of modelling welding processes.

For the thermal-stress analysis, mechanical boundary conditions restraining axial displacements were specified at one end of the finite element model on the tanker shell as shown in Figure G2. The reason for specifying axial restraints at only one end was to simulate the effect of constructing the tanker from end-to-end. For this reason, the transverse residual stress field is very low on the free end (low restraint implies low residual stress) and higher on the restrained end.

4 Results

Von Mises and axial (transverse) stress contour plots are shown in Figure G4. The stress contour plots shown are after cooling. In the bottom frame of this figure, two black arrows indicate the paths along which the transverse residual stress was output. The radial path starts at the root of the weld, at the base of the positioning lip of the extrusion band, and ends at the weld cap. From this figure, it can be seen that the restrained end (the right hand side) exhibits through-wall bending stress, as indicated by the large tensile axial stress on the inner surface of the shell and the compressive axial stress on the outer surface of the tanker shell.

The resulting transverse residual stress profiles are shown in Figure G5. In this figure, the solid curves indicate the actual transverse residual stress as measured from the finite element model. The dashed lines indicate the linearised membrane stress, Qm. This has been calculated as follows: at the root of the weld, define σ_0 =121.15MPa, which is the transverse residual stress

at the root. For a radial position, a, with a = 0 corresponding to the root and a = 5 corresponding to the outer surface of the shell (sub-surface in this case, since a weld cap is present), define σ(a) to be the transverse residual stress at the radial position a. Then the linearised residual membrane stress, Qm(a) is defined by:

$$Q_m(a) = \frac{1}{2}(\sigma_0 + \sigma(a))$$

That is, Qm is the average of the stress at the root and the stress at the radial position a.

Two sets of curves (actual transverse stress and Qm) have been plotted; one for the restrained in and one for the unrestrained end. As expected, the restrained end exhibits higher residual stress than the free end.

5 Conclusions

For a sensitivity study, and to remove the potential over-conservatism of assuming yield-magnitude, tensile residual stresses, it is recommended that the residual stress field specified in this report is employed. Note that at the weld root, the linearised membrane residual stress is equal to 121.15MPa, almost equivalent to the yield stress of the material under consideration. Thus, for shallow defects, the use of Qm is almost equivalent to the assumption of full yield magnitude residual stresses. However, as the defect height increases (and therefore the radial position gets closer to the outer surface of the joint), Qm decreases to be less than 50MPa, or less than half of the yield stress.

Note that the material properties assumed for the welding residual stress simulation will have an effect on the resulting residual stress profile; however, the Qm profile described in this appendix can be used as an indicative profile of potential welding residual stresses in the joint. In particular, as described in the report, the finite element analysis of the welding residual stresses appear to agree will with the experimental measurements over a significant proportion of the joint through-wall thickness.

6 References

Abedrabbo N, Pourboghrat F and Carsley J (2007): 'Forming of AA5182-) and AA5754-O at elevated temperatures using coupled thermo-mechanical finite element models', International Journal of Plasticity, Vol 23, pp 841-875.

AFROX (2014): 'Product Data Sheet: Afrox Filmax 5183 and Afrox TIG 5183', **www.afrox.com**.

efunda (2014): 'Propreties of Aluminium Alloy AA5083', retrieved from **www.efunda.com/Materials/alloys/aluminum/show_aluminum.cfm?ID=AA_5083&show_prop=all&Page_Title=AA%205083.**

GRW (2010): 'Welding Procedure Specification (WPS)', GRW Engineering, 08/02/2010.

GRW (2013): 'Critical crack size & Crack growth estimate – an extended study', GRW Report No. PVVR20121101, Revision 3. Report Date 30 September 2013. Received from DfT via memory stick on Friday, 25/04/2014.

MatWeb (2014): 'ASM Material Data Sheet – Aluminium 5083-H116; 5083-H321', retrieved from http://asm.matweb.com/search/SpecificMaterial.asp?bassnum=MA5083H116,

Summers PT, Case SW and Lattimer BY (2014): 'Residual mechanical properties of aluminium alloys AA5083-H116 and AA6061-T651 after fire', 'Engineering Structures', Vol 76, pp 49-61.

Table G1 Material properties used for the welding simulation

Material Properties	Source	Unit	Temp, °C	Parent metal	Weld metal*
Thermal expansion	(efunda, 2014)	10^{-6}/°C	-	23.4	23.4
Thermal conductivity	(efunda, 2014)	W/mm.K	-	0.120	0.120
Density	(efunda, 2014)	kg/mm^3	-	2.66E-06	2.66E-06
Elastic modulus	(efunda, 2014)	MPa	20	70,000	70,000
			600	7,000**	7,000**
Yield strength	(efunda, 2014) and (Afrox, 2014)	MPa	20	195	125
			600	19.5**	12.5**
Tensile strength	(efunda, 2014)	MPa	20	305, 10% strain	275, 10% strain
			600	19.5	12.5
Specific heat capacity	(Matweb, 2014)	J/kg.°C	-	900	900
Melting point	(Matweb, 2014)	°C	-	591-638	591-638

*Assumed material properties unless stated otherwise
**Assumed 10% of room temperature values

Table G2 Values used to derive the volumetric heat flux

Weld pass	Area (mm^2)	Heat input (J/mm)	Heating period (s)	Heat flux (W/mm^3)
1A	49.22	49.15	3.15	2.6
1B	49.52	49.15	3.15	2.6

Table G3 Additional thermal properties included in the finite element model.

Absolute zero	-273°C
Stefan-Boltzmann constant	5.67·10E-14 W/mm^{2}K^4
Emissivity	0.3
Convective heat transfer coefficient	10^{-5}W/mm^{2}K

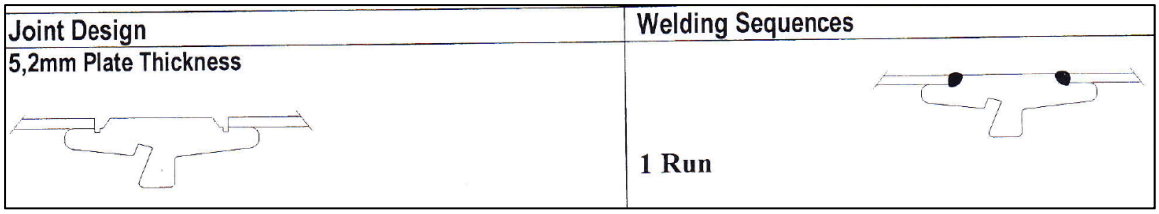

Figure G1 Schematic of the joint under consideration (GRW, 2010).

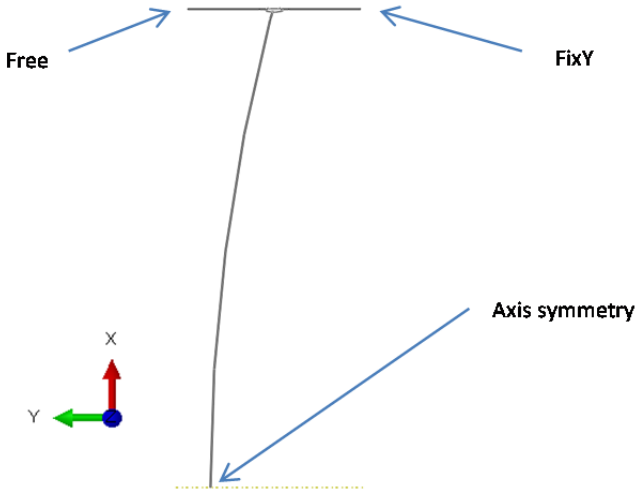

Figure G2 Axi-symmetric cross-sectoin of the welded area.

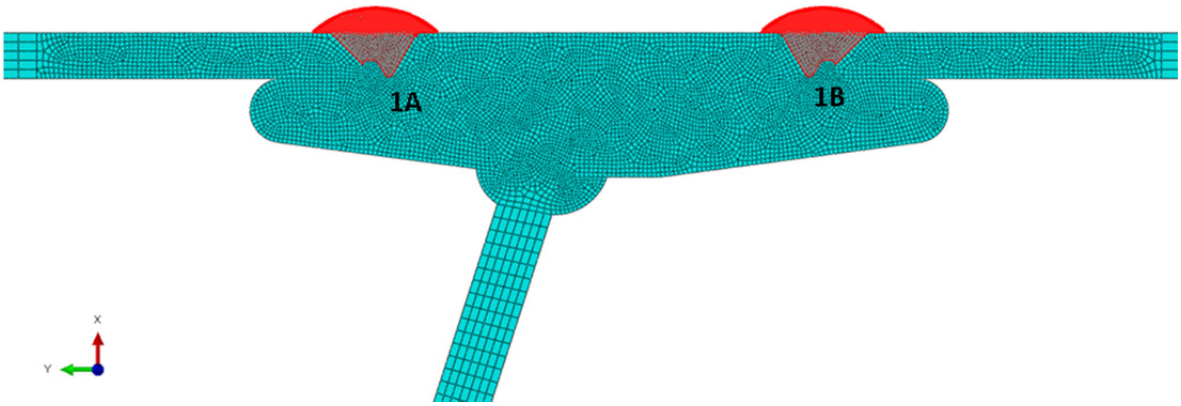

Figure G3 Weld passes. Note that a 'seam' was used to model the unfused surfaces between the tanker band extrusion profile and the tanker shell.

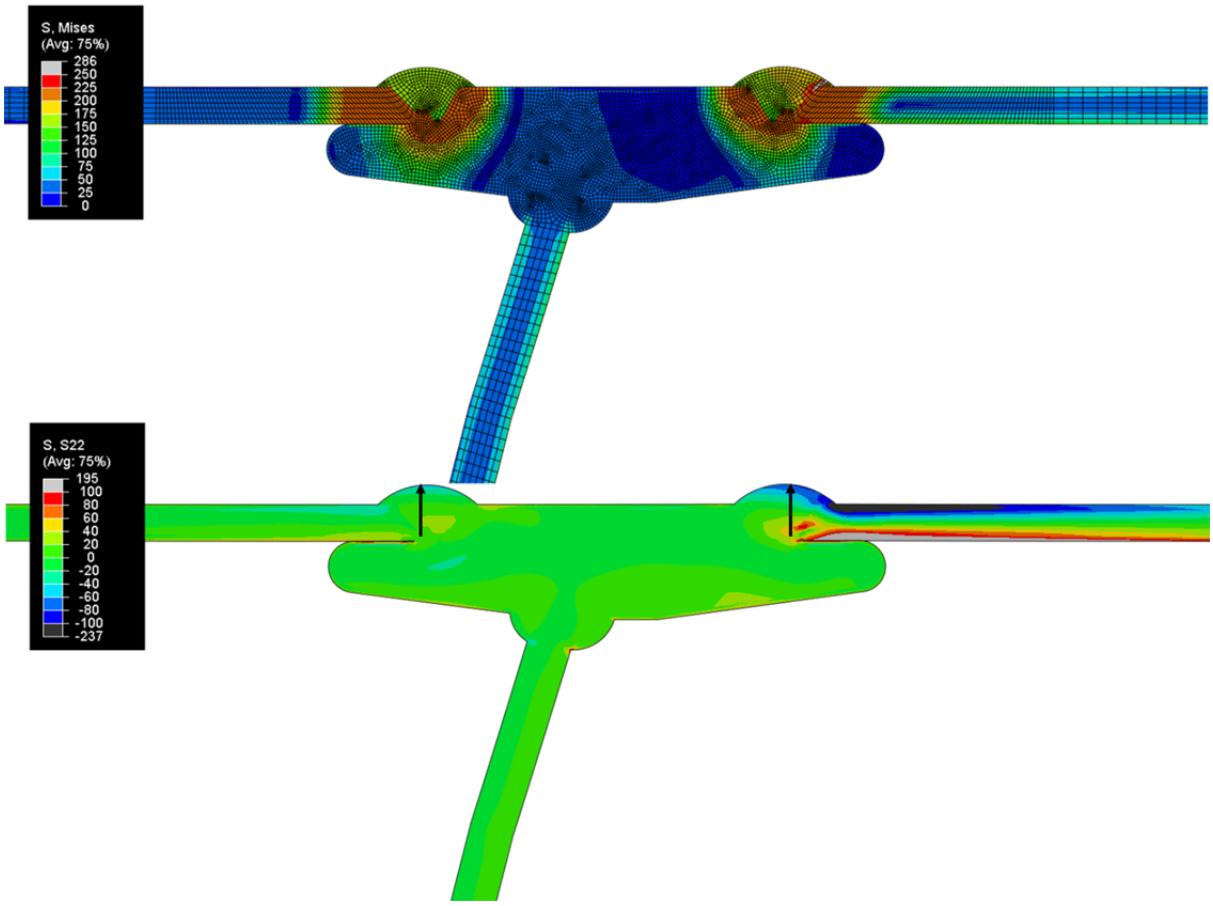

Figure G4 Von Mises stress contour (top) and axial (transverse) stress contour (bottom) for the joint after cooling. The arrows indicate the lines for residual stress measurement.

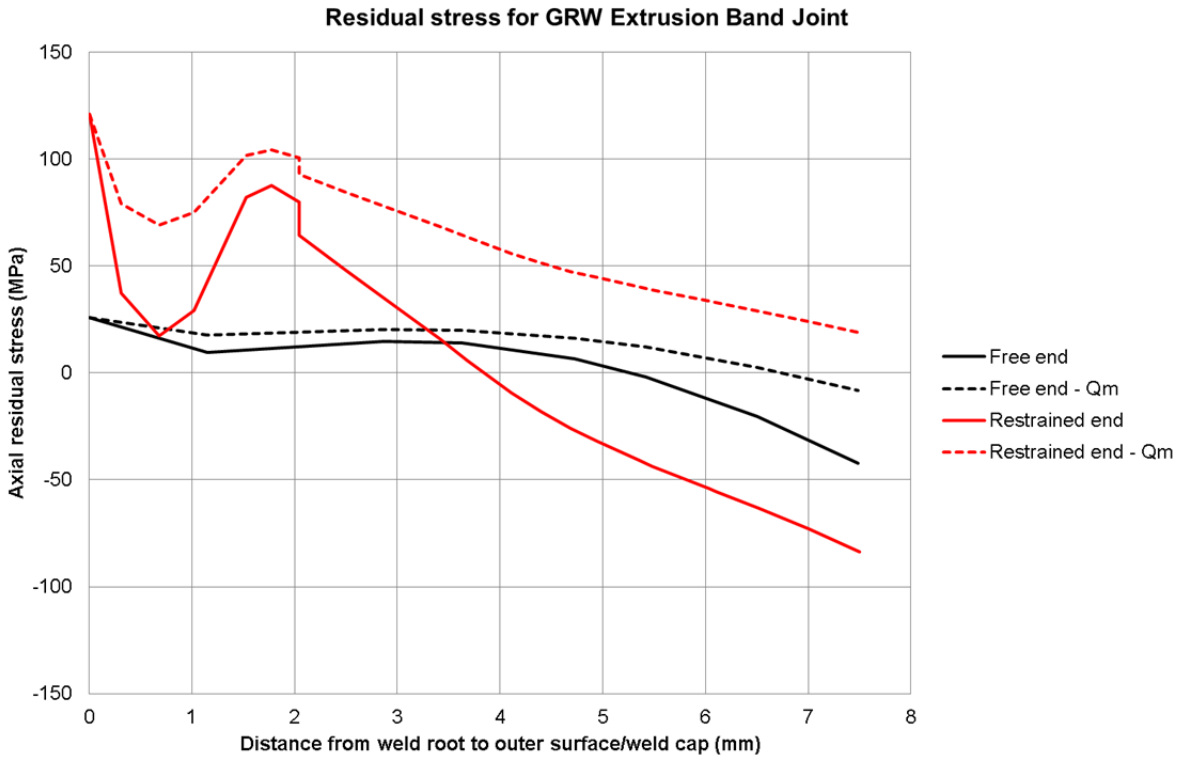

Figure G5 Transverse residual stress profile and resultant linearised membrane stress (Qm).